Available online at www.sciencedirect.com
ScienceDirect
Polymer 48 (2007) 6843–6854
polymer
www.elsevier.com/locate/polymer

Polymer-nanoinclusion interactions in carbon nanotube based polyacrylonitrile extruded and electrospun fibers

Linda Vaisman [a,c], Ellen Wachtel [b], H. Daniel Wagner [c], Gad Marom [a,*]

[a] *Casali Institute of Applied Chemistry, The Institute of Chemistry, The Hebrew University of Jerusalem, 91904 Jerusalem, Israel*
[b] *Chemical Research Infrastructure Unit, The Weizmann Institute of Science, 76100 Rehovot, Israel*
[c] *Department of Materials and Interfaces, The Weizmann Institute of Science, 76100 Rehovot, Israel*

Received 14 August 2007; received in revised form 18 September 2007; accepted 19 September 2007
Available online 17 October 2007

Abstract

Specific interfacial interactions in multi-component systems such as composites improve the chemical compatibility between the filler and the matrix, prevent the filler from aggregating and strengthen the interface. Carbon nanotube (CNT) based polyacrylonitrile (PAN) composites were prepared either by extrusion or electrospinning to yield fibers with diameters on two different scales – micro- and nanometric. Introduction of a third component, ethylene carbonate, a plasticizer which is capable of forming strong dipolar interactions with the nitrile group of the polymer, had a four-fold effect. It enabled melt-processing of the polymer, caused a structural transition in the crystalline matrix, improved the uniformity and decreased the diameter of the electrospun fibers. It also indirectly revealed a preferred interaction between the π-electrons of the CNT and the nitrile groups of PAN, as was identified based on synchrotron microbeam WAXD, DSC, ^{13}C NMR and FTIR of CNT-filled and unfilled PAN fibers. The nature of CNT and PAN interaction was modeled by charge-transfer of CNT π-electrons from the highest occupied molecular orbital to the empty nitrile π* orbital of PAN.

Keywords: Electrospun fibers; Carbon nanotubes; Polyacrylonitrile

1. Introduction

The importance of interfacial properties and stress transfer in classical fiber composite technology has been recognized long ago due to their strong effect on strength, stiffness and fracture toughness of fiber composites in various failure modes [1]. Particularly with respect to nano-reinforcement, the realization of an effective stress transfer mechanism has been the subject of extensive research, in an attempt to achieve disaggregation of the nanosize particles and to improve the dispersion quality [2]. The issue of tailoring of interfacial properties is of utmost importance in view of the extremely large interfacial region typical of composites containing nanofillers.

Carbon nanotubes (CNT) have a unique set of properties that suit them for a wide range of possible applications in suspensions and polymer based solutions, melts and composites [3–6]. Their outstanding characteristics include excellent mechanical properties, high thermal and electrical conductivities, low percolation thresholds and high aspect ratios; this last characteristic provides the nanotubes with an additional advantage over spherical fillers in obtaining advanced composites [7]. On the other hand, large aspect ratios combined with high structural flexibility [8] increase the possibility of nanotube entanglement and close packing [9]. Disaggregation and uniform dispersion are critical challenges that must be met to successfully produce such advanced materials. Various dispersion techniques have been suggested previously in order to overcome the intrinsic van der Waals attraction of carbon nanotubes [10–12]. Our approach relies on the development of interfacial interactions between the π-electronic system of

* Corresponding author. Tel.: +972 2 6585898; fax: +972 2 6586068.
E-mail address: gadm@vms.huji.ac.il (G. Marom).

0032-3861/$ - see front matter © 2007 Elsevier Ltd. All rights reserved.
doi:10.1016/j.polymer.2007.09.032

CNT and the polymer functional groups. This approach was shown to be effective when stable uniform dispersions of carbon nanotubes were obtained with the aid of surfactants having multiple unsaturated carbon bonds [13].

Polyacrylonitrile is not extrudable in a straightforward way because upon heating the polymer tends to char rather than melt. Therefore, a (fugitive) plasticizer, such as ethylene carbonate (EC), has to be mixed with the polymer at low temperatures in order to avoid charring [14]. Due to strong dipolar interactions between the nitrile groups of PAN and the carbonyl (−C=O) groups of the plasticizer, a solvated complex is formed with morphological characteristics that are different from those of the original polymer [15,16]. On their own, the polymeric chains form a rod-like helix due to the intramolecular dipolar repulsion of the nitriles [17]. The nitrile−nitrile interactions also limit the ultimate draw ratio of PAN fibers [18] and control the polymer viscosity [19]. Potentially, the polymer performance, as controlled by the nitrile groups, could be adjusted according to specific requirements by introducing a filler that would interact with the −C≡N groups and consequently reduce the nitrile intrinsic repulsion. Our previous study on multi wall carbon nanotubes (MWNT)−PAN extruded filaments showed that embedding the nanotubes almost doubled the ultimate draw ratio of the filaments and improved the degree of orientation relative to the filament axis [20], effects which were attributed to the newly formed interactions with CNT.

While melt-mixing/extrusion of CNT−PAN composites has been investigated only to a limited extent [20], studies on electrospinning of those composites have been carried out by a number of research groups [21−24]. Among the parameters studied, the electrical conductivity of the solvent was found to be the dominant factor controlling the diameter and uniformity of the electrospun fibers [25]. Ethylene carbonate, known as a fairly conductive reagent ($\sigma \sim 10^{-3}$ S/m), was shown to successfully either wet or dissolve [15] acrylonitrile polymer depending on the polymer−plasticizer ratio. Therefore the dissolution of PAN in EC prior to electrospinning would generally be expected to yield finer fibers with a narrow diameter distribution. Moreover, the polymer morphological transition shown to be induced by melt-mixing of PAN and EC could be tested also in the case of electrospinning.

During melt-mixing with EC, a reversible change occurs in the molecular packing of PAN, namely a hexagonal-to-orthorhombic transition [20,26]. The insertion of a polar additive can ''neutralize'' a fraction of the −C≡N groups [17] and interfere with the intermolecular interactions. Since the forces effective in PAN under stress are believed to predominantly result from intramolecular interactions of the polar −C≡N groups [17], ethylene carbonate will have a strong plasticization effect on PAN, i.e. in its presence the resistance of the polymer fiber to an imposed stress is reduced. As the solvated complex has a different unit cell from that of the original polymer, information on the effect of the filler on PAN could be obtained indirectly by tracking the temperature at which the transition from orthorhombic to hexagonal lattice occurs during heating. The re-establishment of the hexagonal unit cell at comparatively low temperatures would attest to weakening of −C=O and −C≡N dipolar interactions since they are partly replaced by the interactions of nitrile groups with the nanotubes.

This paper aims to monitor the interaction between the π-electrons of CNT and the nitrile groups of PAN by using synchrotron microbeam WAXD analysis of both extruded filaments and electrospun nanofibers. As the orthorhombic structure of PAN relates specifically to the nitrile interactions with EC, we intend to utilize it as a measure of the CNT effect. A comparative morphology−temperature study of PAN/EC and CNT−PAN/EC composites could provide indirect evidence of significant interaction between the π-electrons of CNT and the nitrile groups of PAN. The influence which those interactions have during heating on the orientation of the polymer chain, tacticity, crystal size and glass transition temperature will also be discussed in detail.

2. Experimental

2.1. Materials

Multi wall carbon nanotubes (length: 1−5 μm, diameter: 20−50 nm, nominal purity: 95%) prepared via chemical vapor deposition (CVD; iron-based catalyst, 700−800 °C, acetylene as a precursor) were purchased from NanoLab Inc. (Newton, MA). Polyacrylonitrile ($[C_3H_3N]_n$, $M_w = 150{,}000$) was obtained from Scientific Polymer Products Inc. (Ontario, NY). Ethylene carbonate ($C_3H_4O_3$, purity: 98%) was purchased from Sigma−Aldrich. Dimethylformamide (C_3H_7NO, JT Baker) was used to dissolve the polymer prior to electrospinning.

2.2. Extrusion process

Melt-mixing of EC with 60 wt.% of PAN, or PAN filled with 1 wt.% of MWNT, was carried out in a twin-screw microcompounder (DSM, Netherlands). Mixing was performed at 170 °C for a period of 6 min at 100 rpm, according to the procedure published elsewhere [14]. This was followed by extrusion and drawing of fiber-like filaments with diameters decreasing from 900 to 325 μm and 250 μm for unfilled PAN and CNT−PAN filaments, respectively.

2.3. Electrospinning process

The electrospun PAN hybrid fibers with 0, 1 and 2 wt.% of as received MWNT were prepared as follows. Typically 0.5 g of PAN powder was dissolved in dimethylformamide (DMF) at 90 °C to obtain a 9.5 wt.% PAN−DMF solution. A given weight of nanotubes (0, 5 or 10 mg) was then added to a PAN solution and the nanotubes were dispersed by ultrasonication (Sonics, Vibra-cell) for only 5 min, to avoid the possibility of tube fragmentation. The hybrid fibers obtained had a broad distribution of diameters ranging from 0.3 to 1.2 μm.

To compare the extruded filaments and electrospun fibers, 40 wt.% EC/PAN solutions with and without nanotubes were prepared in a manner similar to that used for unplasticized electrospun fibers. Thus 0.2 g of ethylene carbonate was

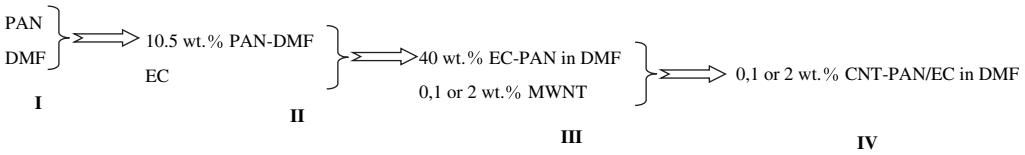

Fig. 1. Four step preparation method of PAN/EC electrospinning solutions with different CNT contents.

dissolved in 10.5 wt.% PAN–DMF solution to eliminate the solution viscosity effect (Fig. 1, II), followed by addition of 0, 1 or 2 wt.% of MWNT (Fig. 1, III) and further ultrasonication according to the method described above.

In a typical electrospun run, a positive high voltage (20 kV) was applied through a copper wire to the solution with a DC power supply (Glassman High Voltage Inc.). The solution was loaded in a plastic syringe equipped with a G32 stainless steel needle (Techcon Systems). The gap (distance between the needle tip and the grounded collector) was kept at 20 cm. The pressure applied to the polymer solution was 0.05 bar. The electrospun fibers were collected on aluminum foil as a randomly distributed fiber mat and left in the hood to remove residual solvent.

2.4. Characterization techniques

2.4.1. Electron microscopy

To investigate the diameter and homogeneity as a function of processing conditions (solution viscosity and conductivity, humidity and CNT content) the electrospun hybrid fibers were viewed with an environmental scanning electron microscope (ESEM, FEG XL30, FEI). To assess nanotube orientation with electrospinning, a high resolution transmission electron microscopy (HR-TEM, Tecnai F20 G^2, FEI) was used to image the as received samples. Note that SEM and TEM images of the extruded fibers were published previously [20].

2.4.2. In situ synchrotron microbeam WAXD analysis

Synchrotron microbeam wide angle X-ray diffraction (WAXD) measurements were performed at the European Synchrotron Radiation Facility (ESRF) on the Materials Science Beamline (ID-11). The X-ray microbeam was monochromatized at a wavelength of 0.5436 Å and collimated to dimensions of 2 μm (vertical) by 50 μm (horizontal). The exposure time for each sample varied from 20 s to 30 s. The extruded filaments were inserted into 0.5 mm or 1 mm diameter Li–glass capillaries (with the sample long axis parallel to that of the capillary). The electrospun nanofibers were randomly wrapped around 0.5 mm diameter capillaries and subsequently inserted into 1 mm capillaries. The samples were mounted in a hot stage (Linkam Scientific Instruments, THMS600, Waterfield, UK). The distance between the sample and the detector was set at approximately 143 mm. Each sample was scanned during heating at 10 °C/min from 25 to ~350 °C. Data were taken at 10 °C intervals. The one-dimensional diffraction profiles were calculated from two-dimensional X-ray diffraction patterns using the image analysis programs Fit2D (ESRF, Dr. Hammersley) and Polar (SUNY, Stony Brook, NY).

2.4.3. Differential scanning calorimetry (DSC)

DSC (Mettler 822^e Toledo, Switzerland) thermograms of the electrospun fibers were measured in the temperature range 25–350 °C at a heating rate of 10 °C/min.

2.4.4. ^{13}Carbon nuclear magnetic resonance (^{13}C NMR) spectroscopy

NMR experiments were carried out at 353 K (80 °C) using a Bruker DRX-400 spectrometer equipped with a BGUII *z*-gradient. The materials (up to 25 mg) were dissolved in deuteriated dimethyl sulfoxide (DMSO-d_6). Typically 1000 scans were accumulated to obtain the spectrum.

2.4.5. Fourier transform infrared (FTIR) spectroscopy

FTIR spectra of the electrospun fibers were measured with an Equinox 55 spectrophotometer (Bruker, Germany). The following parameters were used: DLATGS detector with KBr window, typical scans 64, data analysis by Opus 3.2.

3. Results and discussion

The electrospun hybrid fibers were first visualized by means of scanning and transmission electron microscopy. SEM and TEM micrographs of the extruded filaments were presented and discussed in detail in our previous work [20]. In the case of the electrospun fibers, the addition of ethylene carbonate to the DMF solution of the polymer appears to reduce the average diameter and improve the uniformity as seen in Fig. 2. This results from the higher dielectric constant of the electrospinning solutions generated by partial replacement of PAN with EC [25]. The dielectric constants of the individual components were reported to be 2.7–4.5, 36.7 and 90.5 for PAN, DMF and EC, respectively [25,27,28]. Apparently, the high draw ratios, typically obtained with electrospinning, help to align the nanotubes along the fiber direction (Fig. 3a). However, the overall smooth surface of the electrospun fibers can be altered by curved CNT (Fig. 3b), attesting to good wetting of the nanotubes by the PAN matrix.

Synchrotron WAXD 2-D images were recorded in situ within a selected temperature range for the extruded, drawn, unfilled and CNT-filled PAN filaments. The temperature range was chosen to include the melting (37 °C) and decomposition (from 170 to 245 °C) of the plasticizer [20], as well as the characteristic stabilization process (200–300 °C) of PAN. Extensive research has been devoted in the past to the elucidation of the stabilization reaction of PAN, which results in

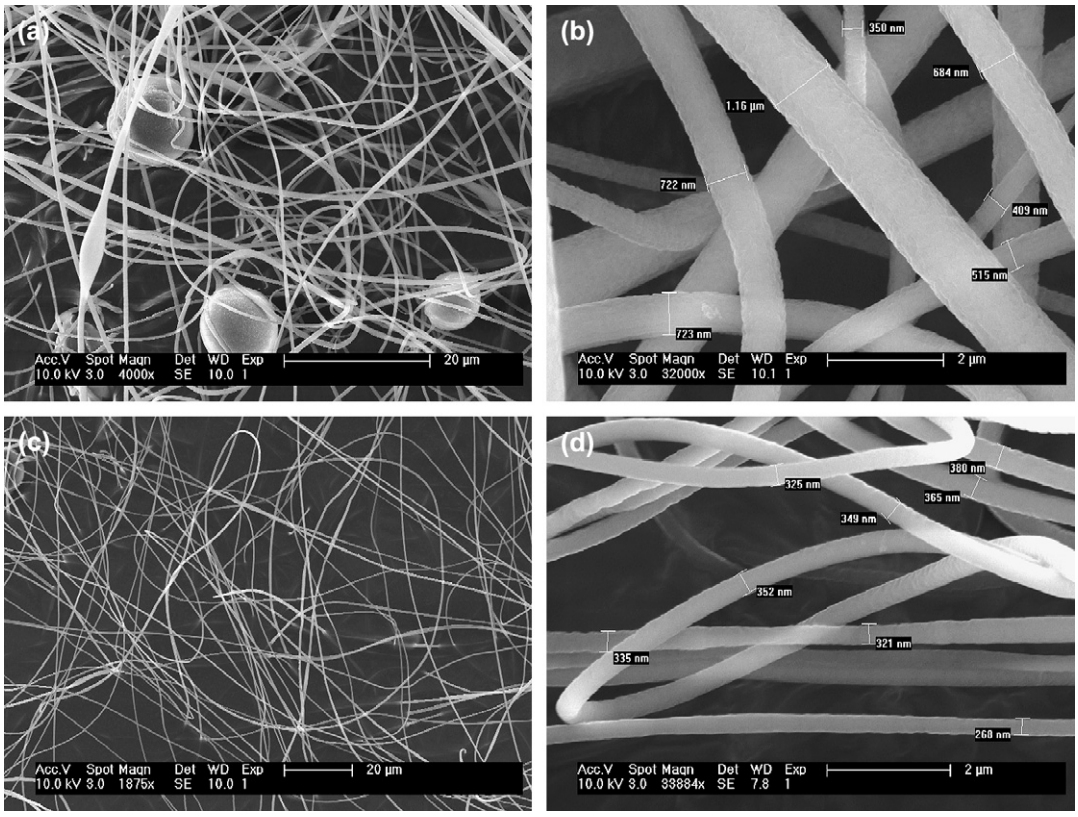

Fig. 2. SEM images of: (a) and (b) PAN electrospun fibers; (c) and (d) PAN/EC electrospun fibers at two different magnifications. Note the improvement in uniformity and decrease in diameter upon addition of ethylene carbonate.

a ''ladder'' structure, formed by cyclization of the nitrile groups [29–32]. These structural changes are expected to be sensitive to the presence of CNT and hence they are of particular interest to this study.

Fig. 4a and b show selected 2-D WAXD images of extruded PAN and CNT–PAN filaments, respectively, with a draw ratio of 5 (an equal draw ratio is essential for valid comparison). The strong diffraction ring corresponds to the doublet $d_{400/220}$, and the weak ring to the d_{620} of the orthorhombic polymorph. An increase in polymer orientation with CNT embedding was previously reported by our group [20] based on comparative analysis of the Herman's factors [18] for unfilled and CNT-filled PAN extruded filaments. The present results support the previously published findings of the effect of CNT on orientation, which is shown here to persist to a higher temperature. Note a minor fiber rotation with heating.

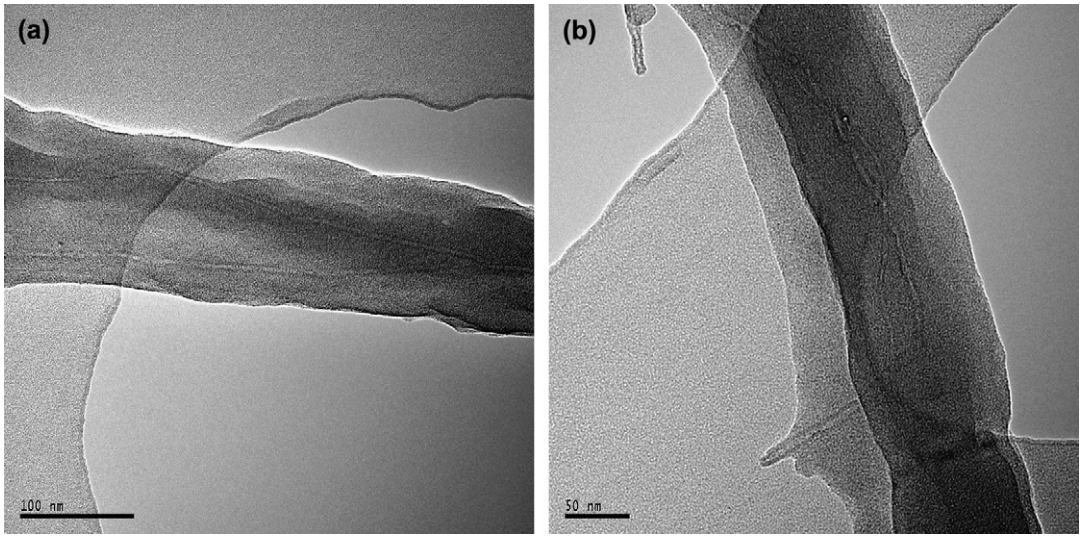

Fig. 3. Transmittance electron microscopy images of 2 wt.% CNT–PAN/EC electrospun fibers supported on a holey carbon film.

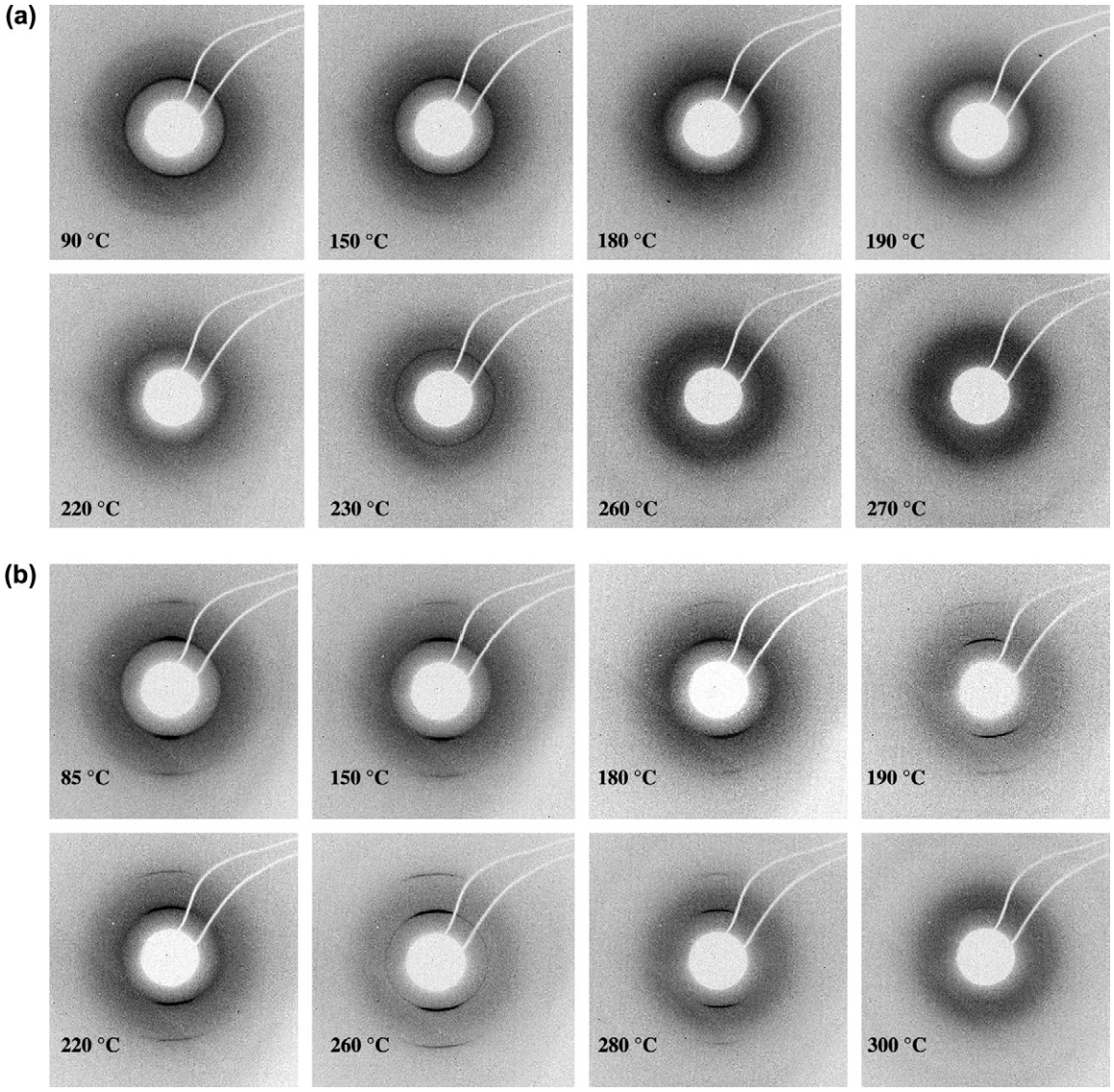

Fig. 4. Selected 2-D WAXD patterns of extruded drawn (a) PAN and (b) 1 wt.% CNT–PAN filaments at different temperatures. The X-ray beam was directed perpendicular to the filament, which was held horizontally. Note a minor fiber rotation with heating. The strong diffraction ring corresponds to the doublet $d_{400/220}$, and the weak ring to the d_{620} of the orthorhombic polymorph.

Heating has a complex effect on the crystallinity of plasticized PAN as the diffraction rings become diffuse twice during the thermal treatment. The final disappearance of the diffraction rings, corresponding to the formation of the ''ladder'' polymer [29], occurs for PAN fibers at 270 °C. Diffraction rings from CNT–PAN fibers disappear at 300 °C. Our previously published DSC analysis of the extruded filaments support this 30 K shift with respect to the temperature measured for PAN fibers [20].

To obtain a better understanding of the structural changes caused by the thermal treatment, 1D histograms of the angular dependence of the diffracted intensity as a function of temperature for filled and unfilled PAN filaments were calculated from the corresponding 2-D WAXD images (Fig. 5). The expected formation of the orthorhombic complex was found with ethylene carbonate and polyacrylonitrile melt-mixing regardless of CNT presence. The characteristic diffraction doublet $d_{400} = 5.3$ Å and $d_{220} = 5.1$ Å appears at $2\theta = 5.8°$ and 6.05°, respectively. The hexagonal crystallinity, typical of the original PAN, is re-formed at a certain temperature as a result of the plasticizer dissociation from the crystals followed by its decomposition. Fig. 5a clearly demonstrates the formation of a noncrystalline intermediate state in the temperature range 180–220 °C for unfilled PAN filaments. The hexagonal lattice, identified by the diffraction peak $d_{100} = 5.3$ Å at $2\theta = 5.8°$, is finally formed at 230 °C. The CNT-filled filaments demonstrate a different behavior with heating (Fig. 5b and c): there is no noncrystalline transition state, and the diffraction at 190° clearly shows the establishment of a hexagonal lattice.

The diffraction patterns of PAN and CNT–PAN electrospun fibers were also recorded during heating and 1D profiles calculated (Fig. 6a and b, respectively), revealing a hexagonal lattice of polyacrylonitrile crystals. For PAN nanofibers the

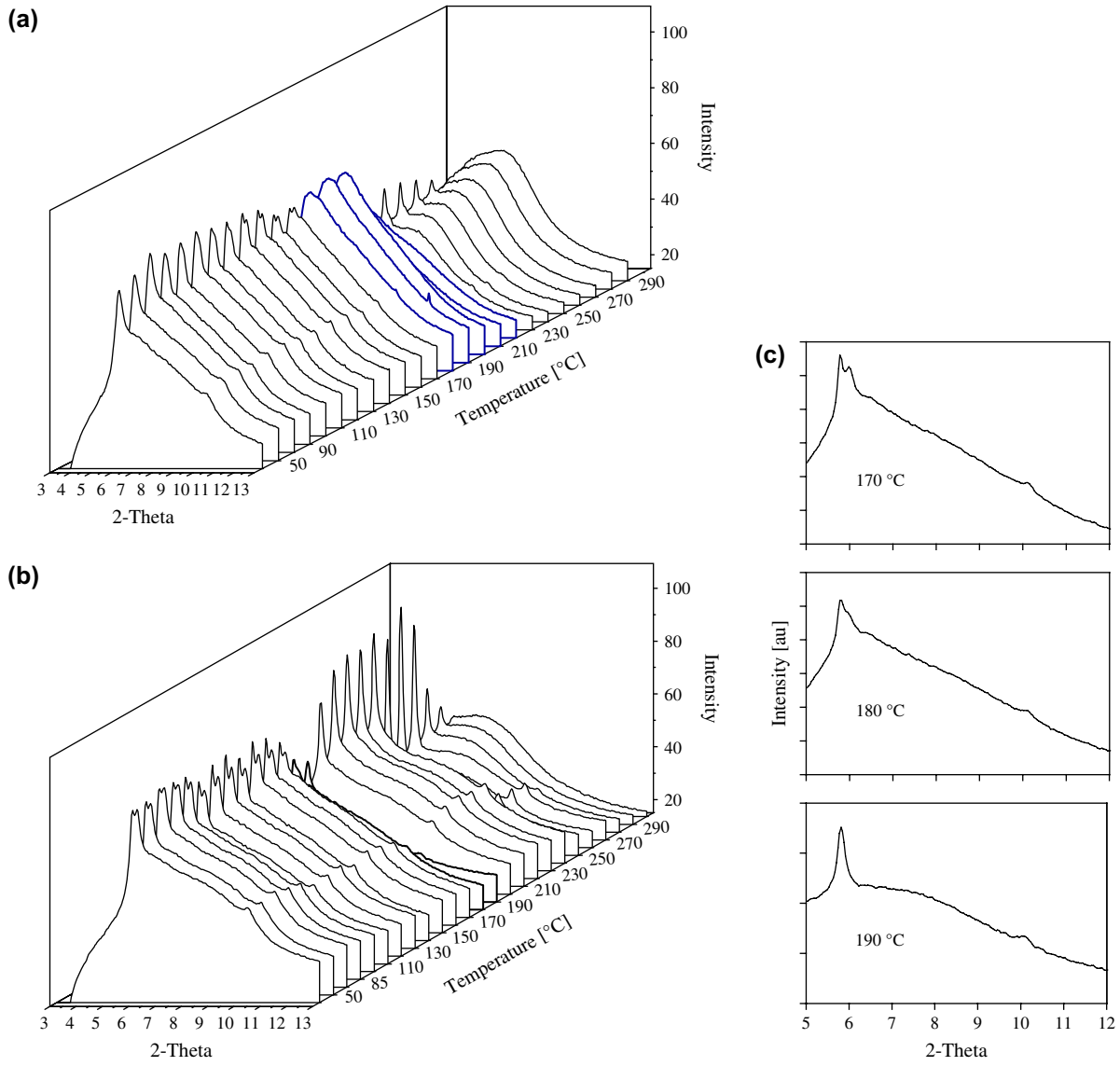

Fig. 5. Histograms of X-ray intensity as a function of temperature for extruded filaments with draw ratio of 5: (a) PAN, the blue lines represent a noncrystalline transition state. Note that due to resolution limitation the doublet could only be detected above 130 °C; (b) and (c) 1 wt.% CNT–PAN.

100 diffraction peak ($2\theta = 5.8°$) is barely detectable at low temperatures (up to almost 80 °C), while the 110 diffraction peak ($2\theta = 9.9°$) is not seen at all, attesting to poor crystallinity in the unfilled samples. In this paracrystalline polymer, line narrowing and intensity increase of the diffraction peaks occur due to larger crystallite size and smaller lattice distortion [33]. Apparently, the crystallite size and perfection of the electrospun fibers increase on heating. The apparent crystallite size (L_c) was estimated by the Scherrer equation, $L_c = K\lambda/B\cos\theta$, where K is the Scherrer constant (to which a value of 1 was assigned [18]), θ is the Bragg angle and $\lambda = 0.5436$ Å is the wavelength of the X-rays. The breadth at half height B was measured in radians from the broadening of the peak at $2\theta_{100} = 5.8°$. The variation of crystallite size with temperature in unfilled and filled PAN nanofibers is plotted in Fig. 7. The graph demonstrates larger crystallite size (L_{100}) for CNT–PAN samples. There is a sharp rise in crystallite size with heating around 100 °C corresponding to the glass transition region of the polymer.

To investigate the effect of EC addition, the diffraction patterns of electrospun unfilled (not shown) and of 1 wt.% and 2 wt.% CNT–PAN/EC fibers were recorded during heating and 1D profiles were calculated (Fig. 8). Apparently, the EC-plasticized electrospun nanofibers do not exhibit orthorhombic crystallinity, and the hexagonal polymorph of the original PAN is preserved. An intense amorphous halo at $2\theta = 7.4°$ probably indicates that the plasticizer is mainly located in the amorphous (disordered) region of the polymer, as opposed to the co-crystallization of EC and PAN in the case of melt-extrusion (Fig. 5). The amorphous halo strengthens with increasing temperature while increasing CNT content has an inverse effect on the amorphous halo intensity.

As mentioned above, the response of the PAN fibers to applied tensile stress depends on the intermolecular interactions

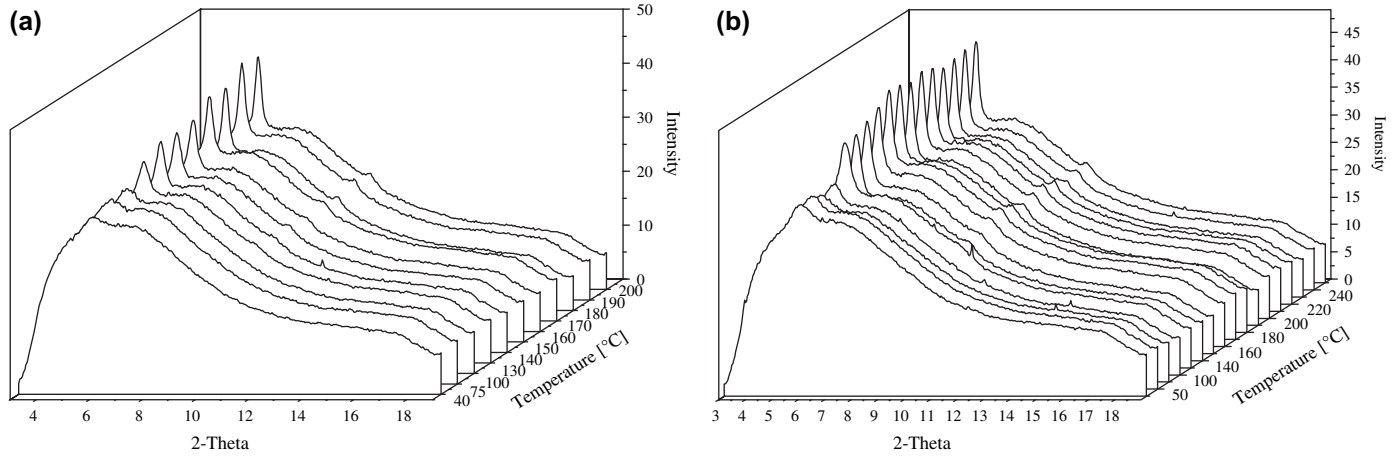

Fig. 6. Histograms of X-ray intensity vs. temperature of electrospun fibers: (a) PAN and (b) 1 wt.% CNT–PAN. The intense diffraction peak corresponds to the d_{100}, and the weak peak to the d_{110} of hexagonal polymorph.

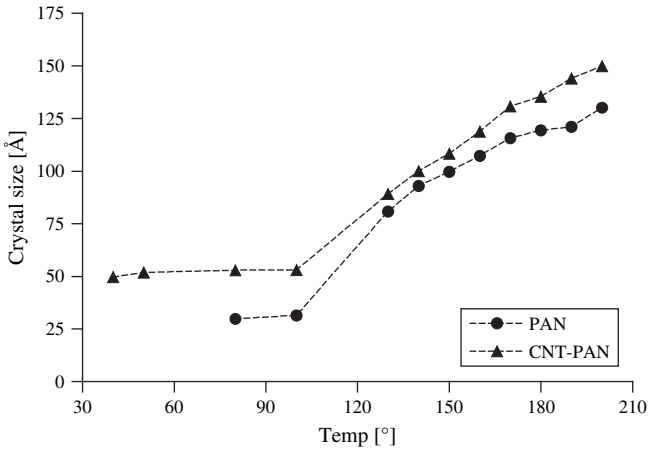

Fig. 7. Crystallite size perpendicular to the {100} planes vs. temperature for CNT-filled (1 wt.%) and unfilled electrospun nanofibers. Note that for the unfilled samples crystallinity was only detectable at 80 °C and above.

of the polar −C≡N groups. Adjacent nitriles of the same macromolecule repel each other. This intramolecular repulsion compels the individual macromolecules to adopt a somewhat irregular helical configuration, fitting within a cylinder of diameter about 6 Å [17]. However, some of the −C≡N groups can extend beyond the boundary of the cylinder, which makes them potentially available for intermolecular dipole–dipole interactions. The insertion of a polar additive and/or CNT can "neutralize" a fraction of the −C≡N groups [17] thereby interfering with the intramolecular interactions, and changing the helix diameter.

A priori, the helix diameter in PAN depends on the draw ratio [26]. Thus, SEM observations (Fig. 2) attest to reduction in electrospun fiber diameter with EC addition probably as a result of increased draw ratio. Measured helix diameter can be correlated with the observed diameter of fibers drawn to a different extent depending on additives. For a hexagonal lattice the helix diameter (D_h) is given by $2d_{100}/\sqrt{3}$ [26]. Fig. 9 shows the change of D_h with temperature for as received PAN powder and a variety of electrospun fibers. The helix diameter decreases with electrospinning, and further narrowing occurs with EC incorporation. The embedding of carbon nanotubes reduces the effect obtained by the plasticizer. The helix diameter increases as a function of temperature, with or without additives, since this is an inherent property of the polymer,

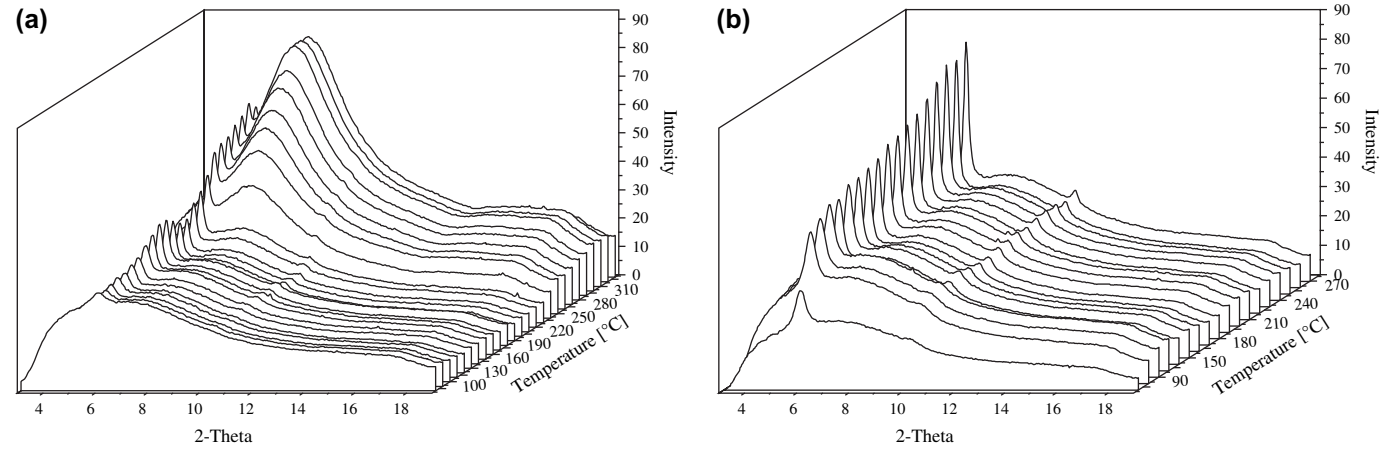

Fig. 8. Histograms of X-ray intensity vs. temperature of EC-plasticized electrospun PAN fibers with different CNT contents: (a) 1 wt.%; (b) 2 wt.%.

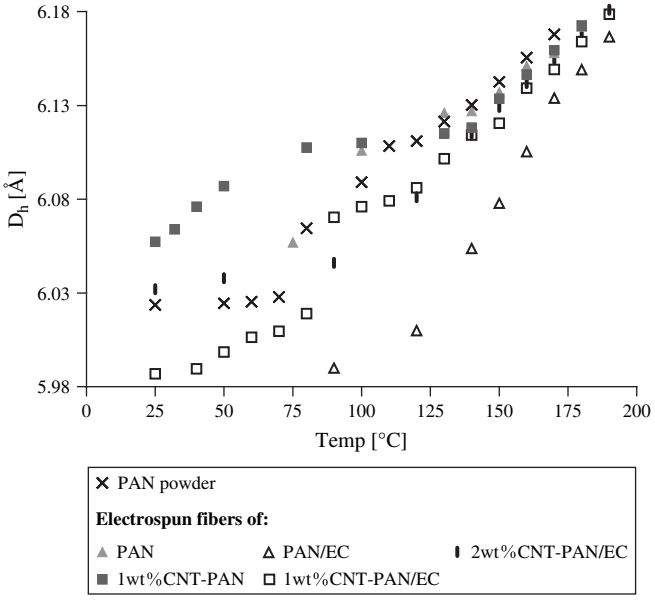

Fig. 9. Change of helix diameter (D_h) with temperature for as received PAN powder and a variety of electrospun fibers.

being related to the lattice spacing increase with temperature [34]. The narrowing effect becomes less important from ~200 °C, partly because the decomposition of EC commences at 170 °C.

As seen from Fig. 9, the helix diameter increases with temperature in a discontinuous way: there are one or two major transition regions, depending on sample type. Previous WAXD studies showed that the lattice spacings of stretched PAN increase in a discontinuous way with temperature [34]. This was taken as evidence that the motions related to the transition in the range 80–120 °C are localized in the more ordered regions of PAN. Commonly the lower glass transition of PAN (around 100 °C) is ascribed to thermal motions of the backbone, while the intermolecular dipole–dipole interactions remain intact at this point. The higher glass transition region (around 140 °C), which sometimes merges with the lower one, is then ascribed to the weakening of the nitrile interactions [17]. DSC analysis of the electrospun fibers was performed to correlate the discontinuous change in D_h with the glass transition temperature (T_g). It is usually found that solvents and plasticizers have a large depressive effect on T_g of PAN [35]. Variation in crystallinity, molecular weight [36], sample form (film or fibers), initiators, comonomers [37] of acrylonitrile polymer may bring further changes in the glass transition temperature.

Electrospinning has a plasticizing effect on the glass transition (Table 1), probably because the measurements were affected by the presence of residual DMF. It is known that removal of solvents, especially those having high dipole moment such as DMF, is difficult in the case of polyacrylonitrile [17]. The traces of the solvent in the electrospun fibers were confirmed by ^{1}H NMR analysis (not shown). The cyclization reaction of nitrile groups was found to occur for CNT-filled electrospun fibers at somewhat higher temperatures than that

Table 1
DSC glass transition temperatures of as received PAN powder and various electrospun fibers (EF)

Sample	T_g [°C]
PAN powder	91, 139
EF PAN	96, 131
EF 1 wt.% CNT–PAN	108, 140
EF PAN/EC	85
EF 1 wt.% CNT–PAN/EC	96
EF 2 wt.% CNT–PAN/EC	110

for the unfilled samples (Fig. 10). This shift was also shown previously for extruded CNT–PAN filaments [20]. The glass transition temperatures are presented in Table 1, showing that with plasticizer addition, the transition at higher temperatures merges with that of the lower region. However, the embedding of carbon nanotubes raises T_g, thereby diminishing the EC-induced plasticization effect.

Finally, tacticity of PAN of the extruded and electrospun fibers was evaluated using ^{13}C NMR spectroscopy in DMSO-d_6 solutions. The practical significance of tacticity rests with its correlation to the physical properties of the polymer. The stereoregularity of the macromolecular structure influences the degree to which it has rigid, crystalline long range order or a flexible, amorphous structure. The tacticity affects the polymer melting temperature, its solubility and even its mechanical properties. Dissolution of isotactic acrylonitrile polymer occurs with difficulty with no evidence of swelling below 90 °C [38]. However, the isotactic configuration is energetically unfavorable compared with the syndiotactic form due to significant repulsive interactions between nearby and parallel –C≡N groups pointing in the same direction [39]. The mechanism of tacticity conversion is proposed in Ref. [40].

^{13}C NMR spectra reflect the differences in the stereoregularity of PAN in the regions of the methine (CH) and nitrile carbons [41,42]. Within the methine carbon region (27–

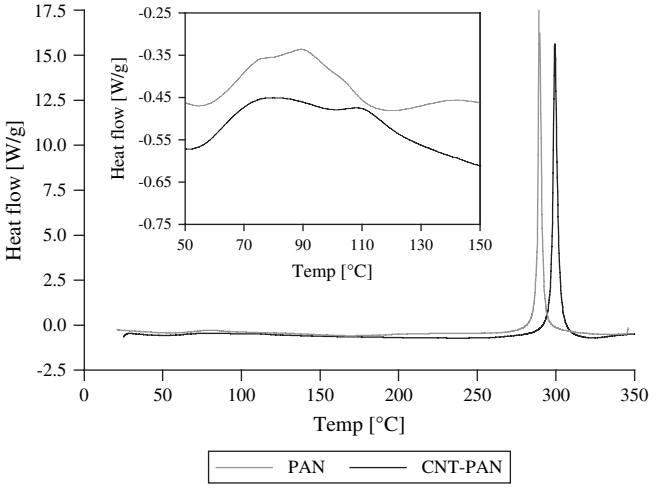

Fig. 10. DSC traces of PAN and 1 wt.% CNT–PAN electrospun fibers, showing the characteristically high exothermic peak of nitrile cyclization reaction around 300 °C; plotted in the inset is a magnified view of the glass transition region.

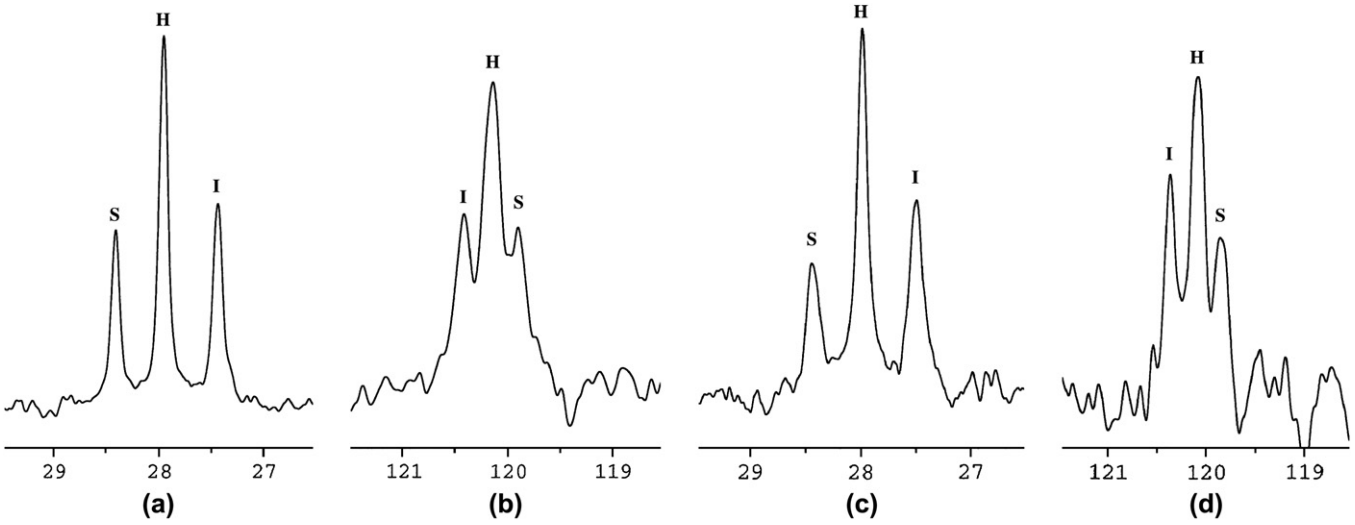

Fig. 11. ^{13}C NMR spectra of PAN (a, b) and 2 wt.% CNT–PAN/EC electrospun fibers (c, d) in DMSO-d_6 at 80 °C: (a) and (c) methine carbon region; (b) and (d) nitrile carbon region. Symbols S, H and I indicate syndiotactic, heterotactic and isotactic triad units.

29 ppm), the isotactic peak appears at a lower magnetic field, while in the nitrile carbon region (119–121 ppm) it appears at a higher field (Fig. 11). In this case isotacticity is determined by three monomer units, denoted triad tacticity. The triad tacticity of various samples is summarized in Table 2 based on the methine carbon spectra.

The measured isotacticity of different PAN samples (Table 2) is in good agreement with values generally obtained by radical polymerization of acrylonitrile [41]. In general, the experimental factors produce only small configurational variations. The embedding of carbon nanotubes into electrospun fibers seems to have a moderate effect on the polymer tacticity: the content of isotactic sequences slightly increases at the expense of both syndiotactic and heterotactic units. The fraction of heterotactic units actually increases with plasticizer addition.

The interaction of the −C≡N group with CNT was also studied by FTIR (Fig. 12). The inset of Fig. 12a demonstrates a small bathochromic shift of the C≡N peak following CNT embedding compared with the neat PAN fiber. The nitrile band, originally appearing at 2248 cm^{-1}, is slightly shifted to 2241 cm^{-1} for 1 wt.% CNT–PAN fibers. Fig. 12b shows FTIR spectra of electrospun plasticized PAN/EC and 2 wt.% CNT–PAN/EC fibers. A few additional features, induced by EC and CNT, can be observed. The C≡N band, which appeared at 2248 cm^{-1} (Fig. 12a), is slightly shifted to 2241 cm^{-1} for both CNT-filled and unfilled plasticized fibers, since the plasticizer and CNT probably shift the nitrile band by the same extent. The presence of the plasticizer EC is demonstrated by two intense peaks at 1800 cm^{-1} and 1774 cm^{-1}. Its high concentration (40 wt.%) and its strong affinity to the nitrile groups probably masks the additional effect of the interaction between CNT and the nitrile groups, based on a shift of the C≡N band. Moreover, the presence of EC seems to have catalyzed some nitrile polymerization, exhibited by the corresponding vibration of the conjugated imine. This vibration at 1596 cm^{-1} is shifted by 30 cm^{-1} towards a lower stretching frequency as a result of carbon nanotube incorporation. This shift can be taken as evidence for interaction between CNT and the conjugated imine system. Since the fibers were not thermally pretreated, and the FTIR spectrum of the unplasticized electrospun fibers (Fig. 12a) shows no evidence of the conjugated structure, it is reasonable to assume that the cyclization reaction of the nitrile groups was initiated by EC. Electrospinning of polyacrylonitrile in the presence of Ag^+ was reported to catalyze the cyclization reactions leading to ladder polymer formation at ambient temperatures [43,44]. It is possible that the formation of strong interactions between the plasticizer carbonyl and the polymer nitrile groups may help to polymerize the nitriles by a similar mechanism.

Table 2
Triad tacticity of as received PAN powder and various fibers – extruded (ExtF) and electrospun (EF) – as measured by ^{13}C NMR. Peak intensity was calculated based on the methine carbon

Sample	Triad tacticity, %		
	S	H	I
PAN powder	22.12	51.38	26.49
ExtF PAN/EC	22.95	49.86	27.19
ExtF 1 wt.% CNT–PAN/EC	19.38	53.59	27.02
EF PAN	21.14	49.56	29.30
EF 1 wt.% CNT–PAN	20.83	46.75	32.41
EF PAN/EC	19.23	54.31	26.46
EF 1 wt.% CNT–PAN/EC	21.32	49.90	28.77
EF 2 wt.% CNT–PAN/EC	20.45	49.73	31.82

4. Mechanism of CNT and PAN interaction

The discussion below addresses the issue of interactions between the π-electrons of CNT and the nitrile groups of PAN with the additional "neutralizing" effect of EC, according to the stated aim of this research.

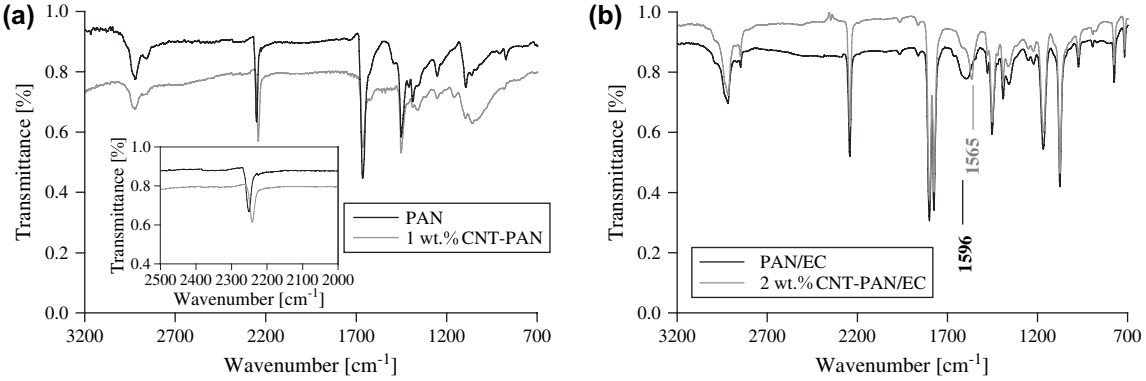

Fig. 12. FTIR spectra of electrospun fibers: (a) PAN and 1 wt.% CNT–PAN; (b) PAN/EC and 2 wt.% CNT–PAN/EC. Note the bathochromic shift of the C≡N and the conjugated C=N–C stretching vibrations due to CNT addition.

It is evident that a strong interaction occurs between –C≡N groups of the polymer and –C=O groups of the plasticizer, promoting the formation of an orthorhombic crystal structure; the original hexagonal crystal structure is recovered upon heat-induced removal of the plasticizer. This reversible transition was also reported for water-plasticized polyacrylonitrile films [26]. The temperature range in which the orthorhombic to hexagonal transition occurs indicates the strength of the intermolecular interactions between –C≡N and –C=O. Accordingly, in the unfilled PAN filaments the hexagonal polymorph is recovered at 230 °C, whereas in the CNT-filled filaments the corresponding temperature is lower by 40 °C. It is suggested that the nitrile–carbonyl interactions are perturbed by CNT, which probably compete with EC by interacting with the –C≡N. The formation of CNT–nitrile interactions was also suggested by our previous study [20]. CNT were found to increase the polymer anisotropy upon drawing and to increase the ultimate draw ratio of the extruded filaments. Carbon nanotube embedding is also shown to increase the crystallite size (L_{100}) of PAN (Fig. 7) and the helix diameter (Fig. 9), and to shift the cyclization to higher temperature (Figs. 4 and 10, and also DSC results published in [20]). All these point to CNT-induced ordering of the crystal structure.

The observed effects of CNT can be explained in the framework of the conventional two-phase structural model of polyacrylonitrile fibers, i.e. a combination of amorphous (disordered) and crystalline (ordered helices) phases [45]. According to this model the nitrile cyclization reaction occurs more readily in the disordered phase that contains fewer –C≡N group pairings [29]. This is compatible with the observed effect of CNT which increases the cyclization temperature by pairing with –C≡N groups and reducing their availability in the disordered phase. In the crystalline phase, where the cyclization reaction is hindered a priori by the close-packed structure, additional hindrance results from the CNT–polymer interfacial interactions. While CNT have a positive effect on the polymer crystallinity and order, the addition of EC facilitates the formation of the disordered phase, reflected in the appearance of an intense amorphous halo in the X-ray diffraction profile (Fig. 10), the lowering of T_g (Table 1) and the increase in the relative amount of heterotactic units (Table 2) in the electrospun fibers.

In view of the experimental results presented we suggest a mechanism to describe the molecular interactions between the –C≡N groups and π-electrons of CNT. One 2s and two 2p atomic orbitals undergo hybridization in graphene, and also in CNT, to form a hybridized sp^2 orbital that has a trigonal planar geometry. These hybridized orbitals form σ bonds between neighboring carbon atoms to produce a hexagonal network of carbon atoms within a graphene sheet. One of the 2p atomic orbitals of each carbon atom overlaps with those of its neighbors to form the π bonding system. It is the delocalization of electrons within the π bonding system that is responsible for the CNT's ability to conduct electricity. Another manifestation of the nomadic nature of the π-electrons of CNT is the π-orbital donation effect of large domains for delocalized electrons [46], expressed by interfacial interactions with potential acceptors.

Probably several different intermolecular forces contribute to the mechanism of CNT π-electron bonding with polyacrylonitrile through its –C≡N groups, such as dispersion and dipole-induced-dipole forces (particularly at long range). Our previous study of extruded PAN filaments by polarized Raman spectroscopy [20] showed that while carbon nanotubes are predominantly aligned with the fiber direction, the orientation of nitrile groups is perpendicular to the fiber axis. This perpendicular orientation could arise from long range dipole-induced-dipole interactions formed between the permanent dipole of the nitrile group ($\mu \approx 4$ D) and the polarizable π-electron density of CNT. Broughton and Bagus [47] showed, for dipoles of finite length, that the interaction is stronger when the negative end (which is the nitrogen atom in the –C≡N group) is closer to the polarizable medium. In analogy to the CNT–PAN system, the polarizability of fullerene tubules was shown to occur due to interaction with the polar HF molecule, resulting in pushing away of the delocalized electrons from the fluorine atoms [48]. On the basis of these observations, we propose here to utilize the molecular orbital (MO) theory for the charge-transfer mechanism, to explain our experimental results and the obtained FTIR spectra (Fig. 12) in particular.

A number of facts pertaining to CNT, relevant to the proposed model, are presented as follows. Depending on how the graphene sheet is rolled up to form a carbon nanotube, the latter can be either a 1D metal or semiconductor [49]. Moreover, the electronic structure of CNT was reported to depend on the tube's length [50] and diameter [51], showing that the band-gap of semiconducting CNT decreases with increasing tube length and diameter. The reactivity of carbon nanotubes was shown to depend qualitatively on the size of the HOMO–LUMO gap (HOMO denotes the highest occupied and LUMO the lowest unoccupied molecular orbital) [52]. These orbitals generally correspond to the occupied and unoccupied π bands near the Fermi level and closely resemble the band structure of graphite. However, the rolling of a graphene sheet into a cylinder interferes with the hybridization of the carbon atoms. The radial states are expected to have a different weight inside and outside the tube, i.e. a different reactivity and polarization of the inner and outer surfaces. Thus, the inner surface of a zigzag (*n*,0) nanotube will likely act as an acceptor and bind donor elements, while the outer surface should have donor properties [52].

With respect to the −C≡N group, theoretical studies of the valence electronic levels of acrylonitrile oligomers are limited to relatively short polymeric chains. Model isotactic and syndiotactic chains with 2,4 and 6 acrylonitrile units were investigated, particularly emphasizing the dependence of π_zCN levels on increasing unit count and polymer tacticity [39,53]. The p_z orbitals contributing to those levels are parallel to the carbon backbone of the chain and the p_z orbitals of two neighboring −C≡N groups interact strongly in the case of isotactic oligomers, leading to a large energy level splitting between the two π_zCN levels [39]. This 2 eV splitting means that the π_zCN levels require longer chain molecules before a converged bandwidth can be claimed, in contrast to πCN and nitrogen lone-pair levels, where the extension of the chain leads to relatively narrow and rapidly converged bandwidths. In the syndiotactic case, owing to the weak interactions between nitrile groups, the corresponding levels display almost no splitting. Having that in mind, the exact energy level diagram of the charge-transfer complex formed from the combination of the highest level of polyacrylonitrile molecule (π_zCN) and π-electrons of CNT will vary in accordance with the PAN unit count, its configuration, and the electronic structure of the tubes, the latter being highly dependant on tube chirality, length, diameter, structural distortion [54] etc.

The role of the −C≡N group as electron donor in the formation of stable electron donor–acceptor complexes with a number of Lewis acids such as BCl_3, $SnCl_4$ and $AlCl_3$ was discussed previously [55]. The donor character of the −C≡N group can arise either from donation of π-orbital electrons of the −C≡N triple bond [56], or the lone-pair localized at the nitrogen atom [57]. For example, the coordination between nitrogen of nitrile group and Ag^+ was recently claimed to yield electrospun PAN fibers with homogeneously dispersed silver particles of nanometric diameter [43,44]. Considering the strong metallic character of CNT, the mechanism of electron transfer from CNT HOMO having e_{2u} symmetry

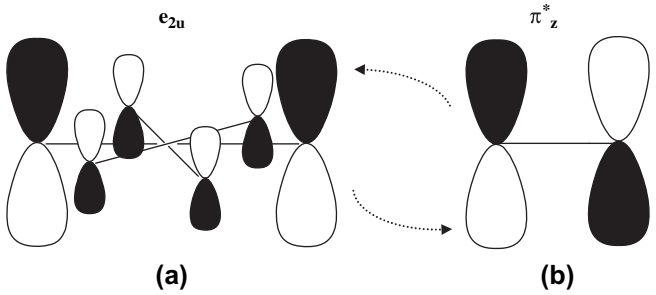

Fig. 13. Schematic correlation diagram of (a) HOMO of carbon nanotubes having e_{2u} symmetry (in agreement with calculations of Bulusheva et al. for an infinitely long tube [52]) and (b) π_z* of −C≡N. The black and white lobes indicate opposite phases of the molecular orbitals.

(according to Bulusheva et al. [52] calculations for an infinitely long tube) into the empty π_z* orbitals on −C≡N (LUMO), seems feasible. Regardless of energy levels, the interaction is favored due to overlapping of symmetry-like orbitals (Fig. 13).

The behavior of the −C≡N group as a π acceptor could be supported by the well known example of carbon monoxide (C≡O), which is able to delocalize electron density from metals with *d* orbitals having local π symmetry [58]. The bonding model fits with trends in C≡O bond lengths and stretching frequencies obtained from FTIR spectra. Populating the carbonyl π* orbital with electrons from metal *d* orbitals results in weakening of the C≡O bond and therefore in a decrease in the stretching frequencies [59]. Accordingly, the observed bathochromic shift in the C≡N (and the conjugated C=N) bond stretching frequency following CNT embedding (Fig. 12) provides the experimental evidence for the occupying of nitrile antibonding orbitals with the π-electrons.

5. Conclusions

The formation of specific interfacial interactions in extruded and electrospun composite fibers of carbon nanotubes as the filler and polyacrylonitrile as the matrix were studied by means of in situ microbeam synchrotron WAXD analysis. Following CNT embedding, the extruded filaments of plasticized PAN were shown to exhibit a polymorphic transition from an orthorhombic to hexagonal crystal structure at lower temperature than in the absence of CNT. This finding corresponds to a weaker intermolecular dipolar interaction between the plasticizer carbonyl and PAN nitrile groups. The carbon nanotubes helped to preserve chain orientation during heating. The crystal size and helix diameter increased with CNT addition, whereas the plasticizer caused helix contraction due to higher draw ratios obtained during electrospinning. While competing to interact with the nitrile groups of the polymer, ethylene carbonate and the filler had an opposite effect on the glass transition of the polymer. Contrary to the amorphous phase intensification found with plasticizer addition, the aligned carbon nanotubes induce growth of more ordered phase in the polymer.

On the basis of the experimental observations a charge-transfer model of π-electron delocalization from carbon nanotube HOMO to the empty nitrile π* orbital was proposed, in analogy to charge-transfer CO–metal complexes.

Acknowledgement

The research was supported by the Israel Science Foundation (Grant # 69/05), and by the (CNT) Thematic European network on ''Carbon Nanotubes for Future Industrial Composites'' (EU), the NOESIS European project on ''Aerospace Nanotube Hybrid Composite Structures with Sensing and Actuating Capabilities,'' and the G.M.J. Schmidt Minerva Centre of Supramolecular Architectures. H.D. Wagner is the recipient of the Livio Norzi Professorial Chair.

References

[1] Kim JK, Mai YW. Engineered interfaces in fiber reinforced composites. Netherlands: Elsevier Science Ltd; 1998.
[2] Ajayan PM, Schadler LS, Braun PV. Nanocomposite science and technology. Weinheim, Germany: Wiley-VCH; 2003.
[3] Assouline E, Lustiger A, Barber AH, Cooper CA, Klein E, Wachtel E, et al. J Polym Sci B 2003;41(5):520–7.
[4] Pötschke P, Fornes TD, Paul DR. Polymer 2002;43(11):3247–55.
[5] Haggenmueller R, Gommans HH, Rinzler AG, Fischer JE, Winey KI. Chem Phys Lett 2000;330(3–4):219–25.
[6] Wang H, Hobbie EK. Langmuir 2003;19(8):3091–3.
[7] Thostenson ET, Li C, Chou TW. Compos Sci Technol 2005;65 (3–4):491–516.
[8] Lourie O, Cox DE, Wagner HD. Phys Rev Lett 1998;81(8):1638–41.
[9] Thess A, Lee R, Nikolaev P, Dai H, Petit P, Robert J, et al. Science 1996;273(5274):483–7.
[10] Hilding J, Grulke EA, Zhang ZG, Lockwood F. J Dispers Sci Technol 2003;24(1):1–41.
[11] Terrones M. Annu Rev Mater Res 2003;33:419–501.
[12] Vaisman L, Wagner HD, Marom G. Adv Colloid Interface Sci 2006;128–130:37–46.
[13] Vaisman L, Marom G, Wagner HD. Adv Funct Mater 2006;16(3): 357–63.
[14] Fishman N. US Patent 5434205; 1995.
[15] Bashir Z, Church SP, Price DM. Acta Polymer 1993;44(5):211–8.
[16] Wang Z, Huang B, Huang H, Xue R, Chen L. J Raman Spectrosc 1996;27(8):609–13.
[17] Henrici-Olive G, Olive S. Adv Polym Sci 1979;32:123–52.
[18] Bashir Z. Acta Polym 1996;47(2–3):125–9.
[19] Atureliya SK, Bashir Z. Polymer 1993;34(24):5116–22.
[20] Vaisman L, Larin B, Davidi I, Wachtel E, Marom G, Wagner HD. Compos A 2007;38(5):1354–62.
[21] Gu SY, Ren J, Vancso GJ. Eur Polym J 2005;41(11):2559–68.
[22] Ye H, Lam H, Titchenal N, Gogotsi Y, Ko F. Appl Phys Lett 2004;85(10): 1775–7.
[23] Kalayci VE, Patra PK, Kim YK, Ugbolue SC, Warner SB. Polymer 2005;46(18):7191–200.
[24] Liu J, Wang T, Uchida T, Kumar S. J Appl Polym Sci 2005;96(5): 1992–5.
[25] Tan SH, Inai R, Kotaki M, Ramakrishna S. Polymer 2005;46(16): 6128–34.
[26] Bashir Z. J Polym Sci B 1994;32(6):1115–28.
[27] Chernyak Y. J Chem Eng Data 2006;51(2):416–8.
[28] Ishida Y, Amano O, Takayanagi M. Colloid Polym Sci 1960;172(2): 129–32.
[29] Ko TH, Lin CH. J Appl Polym Sci 1989;37(2):553–66.
[30] Bashir Z. Carbon 1991;29(8):1081–90.
[31] Warner SB, Uhlmann DR, Peebles LH. J Mater Sci 1979;14(8):1893–900.
[32] Gupta AK, Paliwal DK, Bajaj P. J Macromol Sci Rev Macromol Chem Phys 1991;C31(1):1–89.
[33] Bashir Z. Polymer 1992;33(20):4304–13.
[34] Hinrichsen G. J Polym Sci C 1972;38(1):303–14.
[35] Beevers RB. J Polym Sci Macromol Rev 1968;3(1):113–254.
[36] Beevers RB. J Polym Sci A 1964;2(12):5257–65.
[37] Gupta DC, Agrawal JP. J Appl Polym Sci 1989;38(2):265–70.
[38] Chen H, Liang Y, Wang CG. J Polym Res 2005;12(4):325–9.
[39] Hennico G, Delhalle J, Boiziau C, Lecayon G. J Chem Soc Faraday Transac 1990;86(7):1025–31.
[40] Bashir Z, Manns G, Service DM, Bott DC, Herbert IR, Ibbett RN, et al. Polymer 1991;32(10):1826–33.
[41] Minagawa M, Miyano K, Takahashi M, Fumio Y. Macromolecules 1988;21(8):2387–91.
[42] Inoue Y, Nishioka A. Polymer J 1972;3(2):149–52.
[43] Zhang Z, Zhang L, Wang S, Chen W, Lei Y. Polymer 2001;42(19):8315–8.
[44] Wang Y, Yang Q, Shan G, Wang C, Du J, Wang S, et al. Mater Lett 2005;59(24–25):3046–9.
[45] Gupta AK, Singhal RP. J Polym Sci Polym Phys Ed 1983;21(11): 2243–62.
[46] Dang ZM, Wang L, Yin Y, Zhang Q, Lei QQ. Adv Mater 2007;19(6): 852–7.
[47] Broughton JQ, Bagus PS. J Chem Phys 1982;77(7):3627–34.
[48] Pederson MR, Broughton JQ. Phys Rev Lett 1992;69(18):2689–92.
[49] McEuen PL, Bockrath M, Cobden DH, Yoon YG, Louie SG. Phys Rev Lett 1999;83(24):5098–101.
[50] Rochefort A, Salahub DR, Avouris P. J Phys Chem B 1999;103(4): 641–6.
[51] Niyogi S, Hamon MA, Hu H, Zhao B, Bhowmik P, Sen R, et al. Acc Chem Res 2002;35(12):1105–13.
[52] Bulusheva LG, Okotrub AV, Romanov DA, Tomanek D. J Phys Chem A 1998;102(6):975–81.
[53] Mathieu D, Defranceschi M, Lecayon G, Grand A, Delhalle J. Chem Phys 1993;171(1–2):133–43.
[54] Rochefort A, Salahub DR, Avouris P. Chem Phys Lett 1998;297 (1–2):45–50.
[55] Walton RA. Quart Rev 1965;19(2):126–43.
[56] Bock H, Tom Dieck H. Chem Ber 1966;99(1):213–6.
[57] Purcell KF, Drago RS. J Am Chem Soc 1966;88(5):919–24.
[58] Shriver DF, Atkins PW, Langford CH. Inorganic chemistry. Tokyo: Oxford University Press; 1994. p. 667–9.
[59] Frerichs SR, Stein BK, Ellis JE. J Am Chem Soc 1987;109(18):5558–60.